Nuclear Instruments and Methods in Physics Research A285 (1989) 239–245
North-Holland, Amsterdam

EXPERIMENTAL STUDY OF THE INTERACTION OF AN ELECTRON BEAM WITH THE PONDEROMOTIVE POTENTIAL OF LASER BEATS

Z. SHEENA, S. RUSCHIN, A. GOVER and H. KLEINMAN

Faculty of Engineering, Tel-Aviv University, 69978 Ramat-Aviv, Israel

An experimental setup in which a nonrelativistic electron beam interacts with the ponderomotive potential of two counter-propagating pulsed CO_2 laser beams, operating at different frequencies in a stimulated Compton scattering scheme, was used to investigate various interaction phenomena. The effect of several test parameters on electron trapping and phase area displacement was inspected using a scheme in which electron trapping was achieved by applying a strong abrupt axial dc field along their path. This field is superimposed on a weak axial dc field that is used to separate energetically the trapped electrons from the untrapped ones. In this scheme the effect of the ponderomotive and axial field strengths on the amount of energy exchange between the electrons and the field, and on the fraction of electrons affected was experimentally acquired. The effect of the temporal variation of the laser fields on the interaction was studied using a scheme in which an electron beam intersects the laser beam fields at a small and varying angle. In this scheme the spatial variation of the ponderomotive field resulting from the intersection is seen by the moving electron as a temporal variation of the field. The results of all these tests were processed and compared to the theory, and then used to build a mathematical model that describes the test environment as closely as possible. This model was later applied in a computer program that predicts the collected current from the interacting electron beam after being passed through a low potential drift tube. In the majority of the cases these predictions are identical to the ones measured.

1. Introduction

The quantitative interaction of electrons with the ponderomotive field of an FEL had only been studied theoretically. The present paper describes experiments performed in our laboratory to measure quantitatively some of the relations in such interactions. The quantitative measurement of relations in such a complicated experiment dictated the use of a very complex and precise experimental setup. Such a setup was designed and then built in our laboratory at Tel-Aviv University. Many experiments were then performed with each experiment especially designed to measure the required effect. In parallel theoretical analysis simulating the environment of the experiment was performed in order to predict the results and also in order to use them for comparing and judging the accuracy of the test results.

2. Theory

The governing equation of motion of an electron in a ponderomotive field is the axial force equation [1,2]:

$$\frac{\mathrm{d}(\gamma m v)}{\mathrm{d}t} = -eE_{\mathrm{ac}}(z) - eE_{\mathrm{p}}\cos\{(\omega_{\mathrm{s}}-\omega_{\mathrm{w}})t-(k_{\mathrm{s}}+k_{\mathrm{w}})z\}, \tag{1}$$

where E_{ac} is the externally applied axial field, ω_{s}, k_{s}, ω_{w}, k_{w} are the angular frequency and the wave number of the signal and the wiggler beams, and E_{p} is the ponderomotive field given by:

$$E_{\mathrm{p}} = \frac{e\sqrt{\mu/\epsilon}}{\gamma_{\mathrm{r}} mc^2}(\lambda_{\mathrm{s}}+\lambda_{\mathrm{w}})\,|\hat{e}_{\mathrm{s}}\cdot\hat{e}_{\mathrm{w}}|\,\frac{\sqrt{P_{\mathrm{s}}P_{\mathrm{w}}}}{\pi^2 w_{\mathrm{s}} w_{\mathrm{w}}}. \tag{2}$$

$\hat{e}_{\mathrm{s}}$, $\hat{e}_{\mathrm{w}}$, P_{s}, P_{w}, w_{s}, w_{w} are the polarization unit vectors, powers and waists of the signal and wiggler waves respectively. The resonance electron velocity v_{r} is given by:

$$v_{\mathrm{r}} = \frac{\omega_{\mathrm{s}}-\omega_{\mathrm{w}}}{k_{\mathrm{s}}+k_{\mathrm{w}}} \tag{3}$$

and the resonance phase ψ_{r} is given by

$$\psi_{\mathrm{r}} = \sin^{-1}\left(\frac{E_{\mathrm{ac}}}{E_{\mathrm{p}}}\right). \tag{4}$$

2.1. Trap depth

The trap depth for $E_{\mathrm{ac}}/E_{\mathrm{p}} \ll 1$ is given by

$$\delta\gamma = 2\beta\sqrt{\frac{mc^2E_{\mathrm{p}}}{e(k_{\mathrm{s}}+k_{\mathrm{w}})}}. \tag{5}$$

For $E_{\mathrm{ac}}/E_{\mathrm{p}}$ close to unity the trap depth $\delta\gamma_{\mathrm{a}}$ can only be calculated numerically. Fig. 1 shows a plot of the ratio of the actual trap depth at a finite axial field $\delta\gamma_{\mathrm{a}}$ to the trap depth at zero axial field $\delta\gamma$ (given by eq. (5)) as a function of $E_{\mathrm{ac}}/E_{\mathrm{p}}$.

0168-9002/89/$03.50

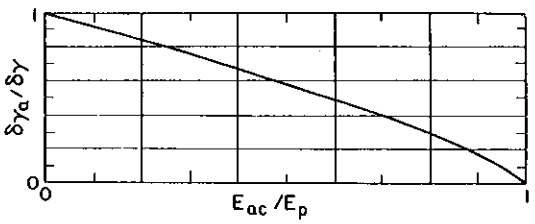

Fig. 1. Ratio of the actual trap depth to the maximum depth as a function of the ratio of the axial field to the ponderomotive field.

2.2. Trapping fraction

A numerical solution of eq. (1) can be used to calculate the trapping fraction for a known trapping mechanism. The results of such a solution for the case where trapping was achieved by applying a strong and abrupt axial field [3] is depicted in fig. 2. In this figure the trapping fraction is given for the parameters given in table 1 as a function of the initial energy relative to resonance of a monoenergetic electron beam. The periodic behavior of the curve in fig. 2 is explained in an accompanying paper in this special issue. For a hot beam the trapping fraction can be calculated as follows by integrating the phase space distribution of the electron beam within the borders of the separatrix:

$$T = \sqrt{\frac{2b}{\pi}} \int_{-\pi}^{\pi-\psi_r} \int_{0}^{F_s(\psi)} e^{-bu^2/2}\, du\, d\psi, \tag{6}$$

where F_s can be approximated by the separatrix function

$$F_s = \delta\gamma_a \sqrt{\tfrac{1}{2}\left(\cos\psi_r + (\psi + \psi_r - \pi)\sin\psi_r + \cos\psi\right)}, \tag{7}$$

u is the electron energy and b is the electron energy

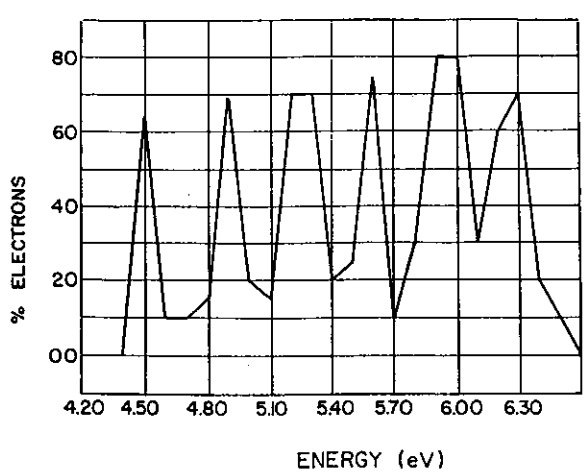

Fig. 2. Electron trapping efficiency vs the relative electron energy using an abrupt axial field of 1000 V/m.

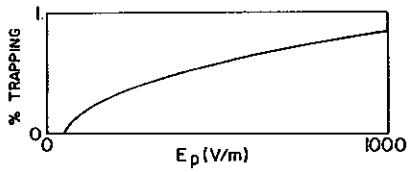

Fig. 3. Trapping fraction as a function of the ponderomotive field.

spread. Fig. 3 gives values of T that were calculated numerically as a function of E_p.

2.3. Field pulse model

In our experiment the ponderomotive field is a function of the laser fields which are obtained from two pulsed TEA CO_2 lasers. A laser pulse shape that matches the pulse shapes measured experimentally can be modelled using the following function:

$$p(t) = a_1 t^7\, e^{-(\ln t)^{a_2}}, \tag{8}$$

where a_1, a_2 are constants that are used to match the pulse width and tail shape and t is the time measured in nanoseconds. Fig. 4 gives a pulse shape for $a_1 = 5 \times 10^{-7}$ and $a_2 = 1.87$. Two laser pulse functions $p_1(t)$ and $p_2(t)$ can be used to calculate the resulting ponderomotive field E_p as a function of time:

$$E_p(t) = E_{pmax}\sqrt{p_1(t)\,p_2(t)} \tag{9}$$

and the trap depth $\delta\gamma_a$ can be approximated using a straight line function that matches the function calculated numerically and shown in fig. 1 as follows:

$$\delta\gamma_a(t) = \delta\gamma_{max}\left(1 - \frac{E_{ac}}{E_p(t)}\right). \tag{10}$$

Fig. 5 shows two laser pulses together with the resulting ponderomotive field pulse $E_p(t)$ and the trap depth pulse $\delta\gamma_a(t)$.

2.4. Temporal effects

Electrons can get trapped inside a ponderomotive field that rises with time as shown in fig. 6. It can be seen from this figure that the energy range of trapped

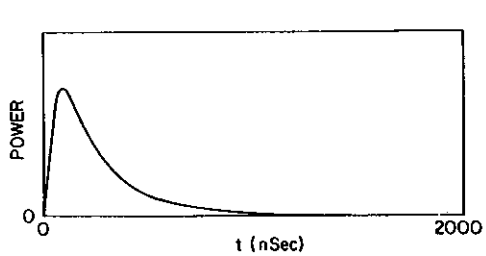

Fig. 4. Approximation of the laser pulse shape.

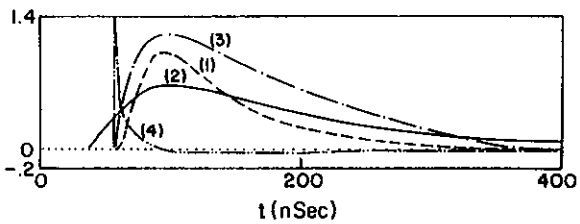

Fig. 5. Laser pulses (1, 2), trap depth pulse (3), and time derivative of trap depth pulse (4).

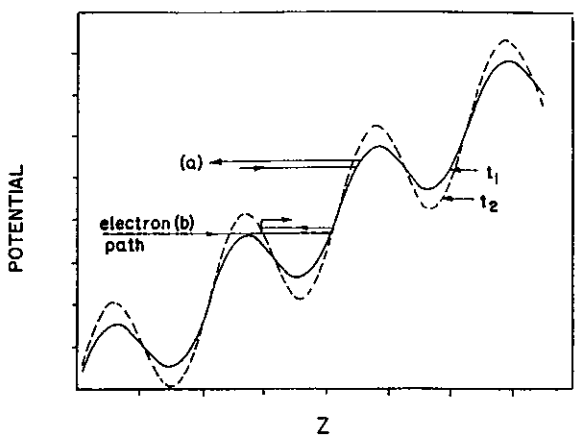

Fig. 6. Electron conservation of energy diagram.

electrons is a function of their synchrotron oscillation time T_{syn} and the gradient of the field represented by the rise of the trap depth $d\delta_\gamma/dt$. The energy range of electrons that get trapped between γ and $\gamma + \delta\gamma$ correspond to electrons for which the potential barrier grows within one synchrotron oscillation time by $(d\delta\gamma/dt)T_{syn}$, so that they find the potential barrier of the wall open upon entrance and closed upon exit after a full synchrotron:

$$\Delta\gamma = \frac{d\delta\gamma_a}{dt} T_{syn}, \tag{11}$$

where

$$T_{syn} = 2\pi\sqrt{\frac{m}{eE_p(k_s + k_w)}}\,. \tag{12}$$

3. Experiment

3.1. Experimental setup

In the experiment we used two intense TEA CO_2 laser beams with wavelengths of 10.6 and 9.3 μm for the wiggler and the signal fields. Special techniques were used in order to make the lasers generate pure monochromatic signals [5]. Both beams are pulsed (about 150 ns) and are synchronized with each other. They interact inside the test tube with an electron beam that is guided along the tube using a strong static axial magnetic field generated by passing a 400 A current pulse through a copper coil surrounding the electron beam as shown in fig. 7. The electrostatic potential was varied along the tube as shown in fig. 7b by using a combination of two effects: the uniform moderate axial decelerating field of 55 V/m is generated by the ohmic potential drop associated with the 400 A current pulse through the copper coil; the abrupt potential drop at location e in fig. 7a is generated by two closely spaced hollow electrodes which are biased by an external dc power supply. After the interaction the electrons are decelerated, bent and guided along a drift tube biased at low potential (about 10 eV). The drift tube serves as an energy analyzer dispersing the trapped electron current signal in time. Electrons that acquire energy from the radiation field during the laser pulse period move faster in the drift tube and appear in the collector as a negative current signal of excess electrons followed by a positive current signal of electrons deficiency, and vice versa for electrons that lose energy to the radiation field. The collected electron signal and the laser pulses are acquired by a real time computer using three high speed digital recorders. (See table 1 for details on the experiment parameters.)

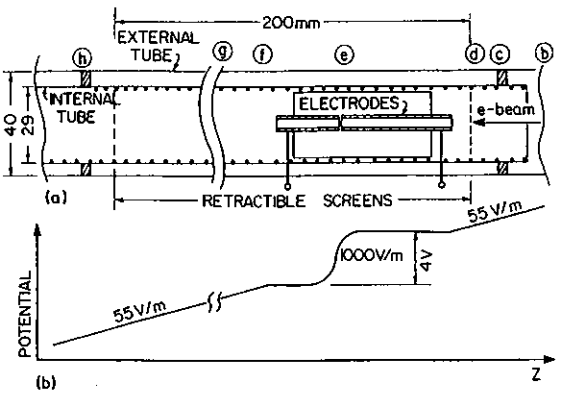

Fig. 7. Experimental tube (a), potential along the tube (b).

Table 1
Parameters of the experiment

Signal power	450 kW
Wiggler power	250 kW
Signal wavelength	9.2938 μm
Wiggler wavelength	10.591 μm
Laser beam waist	0.9 mm
Coil current	400 A
Axial electric field	55 V/m
Electron current	7 μA
Resonance energy	1088 eV

3.2. Field measurement

We used the fact that the trapping drops to zero, when the ponderomotive field has the same value of the axial field (as shown in fig. 1), to measure the true axial field in the interaction region. The measurement was done by lowering the intensity P_i of one of the laser beams to a level P_0 where trapping ceases; then the ponderomotive field at power level P_i is calculated using the following relation:

$$E_p = E_{ac}\sqrt{\frac{P_i}{P_0}}, \tag{13}$$

where E_{ac} is the dc axial field and the ratio P_i/P_0 can be calculated from the detector signals. In our experiment the ponderomotive field calculated this way was around 600 V/m compared to 620 V/m calculated using eq. (2).

3.3. Trapping fraction measurement

The trapping fraction is calculated from the ratio of the trapped electron current to the dc current emitted by the electron gun. Trapping conditions are set experimentally by adjusting the e-beam velocity, to synchronize exactly at the location of the electrodes (item e in fig. 7), where they experience an abrupt potential change, and are injected into the traps. A decelerating axial field applied by the potential drop along the coil separates the trapped and the untrapped electrons in the energy domain. The trapped electron current is measured after separating the trapped electrons from the untrapped ones using a retarding electrode set at zero potential at the end of the interaction region and at the entry to the drift tube. Only electrons which obtained energy from the radiation field (namely trapped electrons) go through the electrode and enter the drift tube. The electrons are then transported through the drift tube at a moderate energy up to the collector. The current from electrons that experienced phase area displacement was measured

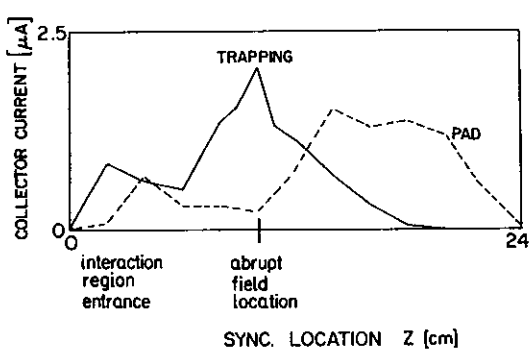

Fig. 8. Electron trapping (a) and PAD (b) current as a function of synchronization location.

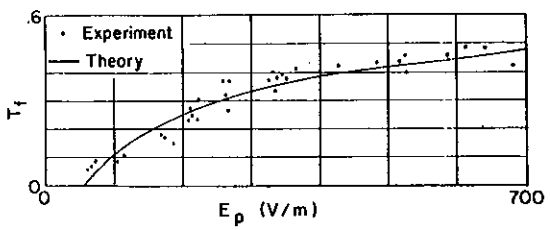

Fig. 9. Experimental and theoretical relation between the trapping fraction and the ponderomotive field.

in a similar way except that an accelerating axial field was applied along the interaction region instead of the decelerating axial field in the case of trapping measurement. Fig. 8 shows measurements of the electron current accelerated by the beat wave (passing through a retarding electrode of 0 V) drawn as a function of the synchronization location (where $v_z = v_{ph}$) along the interaction region. Curve (a) corresponds to a decelerating field in the interaction region where the electrons acquired energy by the trapping process. Curve (b) corresponds to an accelerating field where the electrons obtained energy by the PAD process. From this figure it can be seen that the trapped electron current is maximal at the point where the abrupt axial field is applied, while PAD current is minimal. Also it can be noticed that PAD current is maximal at points where the trapping mechanism did not exist. Trapping and PAD effects were also measured as a function of the ponderomotive field. Changing the ponderomotive field was achieved by exploiting the long tail of the laser pulses as shown in fig. 4. Allowing a variable delay between the laser pulses permits to generate a ponderomotive field with a variable strength without changing the size and the focussing characteristics of the laser beams. Measurements of trapping efficiency as a function of the ponderomotive field are given in fig. 9.

3.4. Electron energy distribution

A variable retarding potential was applied on the electrons emerging from the interaction region passing through the electrode at the entry to the drift tube in

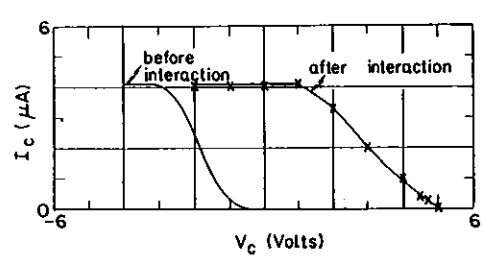

Fig. 10. Electron current as a function of electron energy before and after trapping.

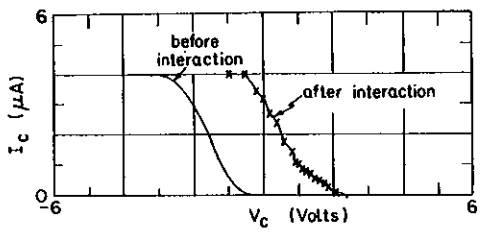

Fig. 11. Electron current as a function of electron energy before and after PAD interaction.

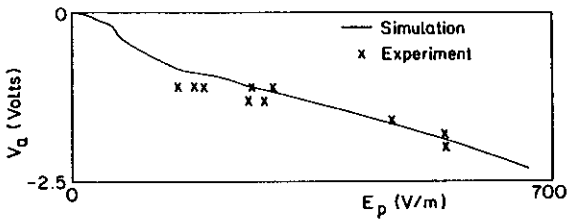

Fig. 13. Experimental and theoretical relation between PAD average energy shift and the ponderomotive field.

order to measure the current of the electrons having an energy higher than the electrode potential. The trapped electron energy distribution shown in fig. 10 was measured when a decelerating axial electric field was applied along the interaction region, while the energy distribution of electrons experiencing PAD shown in fig. 11 was measured while applying an accelerating axial field. Energy distribution of the trapped electrons was also measured for a varying ponderomotive field. Decreasing the strength of the field decreased the maximum energy shift of the electrons. This effect is due to detrapping occurring along the interaction region. As can be seen from fig. 12, the lower the ponderomotive field the higher this detrapping effect. We also measured the average the shift in the energy distribution of the electrons due to PAD as a function of the ponderomotive field (fig. 13).

3.5. Drift tube characteristics

The energy distribution of the electrons emerging from the interaction region can be measured also by measuring their time of flight in the low potential drift tube. The drift tube characteristics were measured by injecting a short current pulse at the electron gun and then measuring the delay in time for different drift tube potentials. These measurements were later used to obtain an empirical relation between electron energy and delay time:

$$t_d = \frac{1200}{\sqrt{V - V_d - 1.03}} + 55, \qquad (14)$$

where t_d is the delay time in nanoseconds, V is the electron energy in eV and V_d is the drift tube potential in volts.

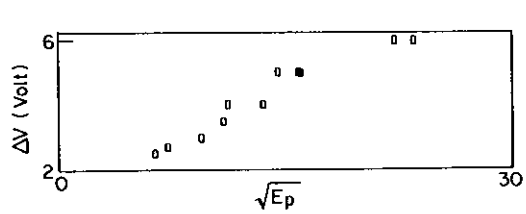

Fig. 12. Electron energy shift as a function of the ponderomotive field in a trapping type of interaction.

3.6. Effects of temporal and spatial variation of fields

As explained in section 2.4, a rising ponderomotive field can cause electron trapping. For the pulse duration of about 150 ns that we used in our experiment this effect is small and it is very difficult to separate it from other trapping mechanisms. In order to enhance this mechanism we modified our setup in order to generate spatial variation in the amplitude of the ponderomotive field, which is equivalent in the electron frame to temporal variation of the pulse. This was done by making one of the laser beams intersect the other beam and the electron beam with a very small angle. As can be seen from fig. 14 the field as viewed by the electron beam has a spatial pulse shape. Due to the speed of the electron the duration of this pulse is very short and is around 10 ns which is much smaller than the duration of the laser pulses. Another advantage of this scheme is that it is possible to make the electrons resonate at different points along the pulse. Making the electrons resonate at a point on the leading edge of the pulse caused a trapping effect with a trapping fraction that is a function of the angle between the beams. The bigger this angle the stronger the trapping effect. On the other hand resonance at the trailing edge of the pulse caused a PAD effect that was independent of the angle between the beams.

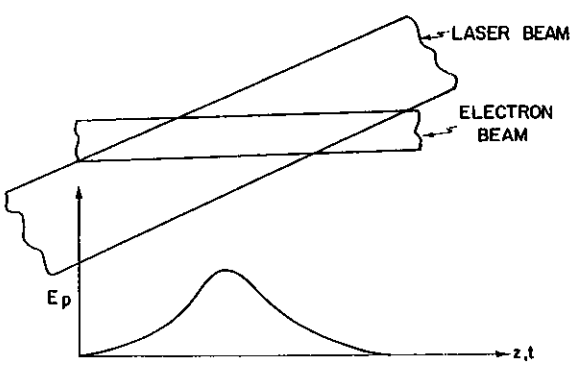

Fig. 14. Spatial distribution of ponderomotive field resulting from two laser beams with a small angle between them.

4. Comparison between theory and experiment

In the following subsections we present some of the test results together with the results obtained from theory and numerical simulations.

4.1. Trapping

Two main trapping characteristics are considered here: The first one is the shift in the energy of the trapped electrons. Fig. 10 shows that the difference in the energy of the electrons before and after the interaction is about 6 eV. This is consistent with a theoretically predicted shift of 6 eV corresponding to the work done by an electron experiencing an axial field of 55 V/m along the interaction length of about 11 cm. The second measured characteristic to be compared with the theoretical model is the trapping fraction as a function of the laser beam fields. This dependence is a very complex function of many experimental parameters such as the trap depth, the axial electric field and the energy distribution of the electrons before the interaction. Fig. 9 shows the trapping fraction as a function of the ponderomotive field as measured in the experiment compared with the same parameter as predicted by eq. (6) using the measured ponderomotive field and the measured energy distribution of the electrons emerging from the electron gun. All the above mentioned comparisons reveal that the consistency between the experimental data and the model dependent predictions is excellent.

4.2. PAD

The main properties of PAD are the change in the energy spread of the electrons and the average shift in the energy of the electrons as a function of the ponderomotive field. From fig. 11 it can be seen that the average electron energy shift is about 2.2 eV as compared to a value of 2.3 eV predicted by numerical simulation using the maximum measured ponderomotive field of 600 eV. Comparison between experimental data and simulation of the energy shift as a function of the ponderomotive field is shown in fig. 13.

4.3. Collected current pulse

A computer program that uses the measured experiment parameters starting from the measured laser pulse shapes, including the measured electron trapping and PAD characteristics through the measured electron transport properties in the drift tube, were used to predict the collected current from an electron beam that interacted with the ponderomotive field. The program numerically simulates the motion of 35000 electrons having an initial Gaussian energy distribution with the measured distribution width of 2.5 eV, then experiencing a time dependent energy shift with the measured properties of either trapping or PAD as defined by the

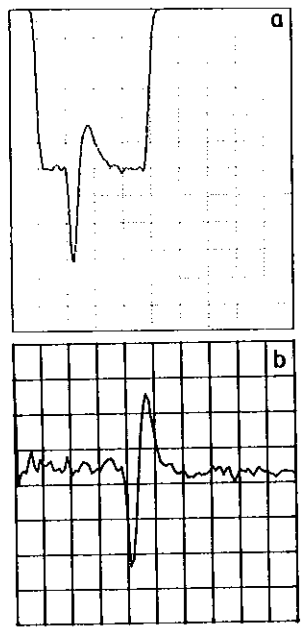

Fig. 15. Theoretical (a) and experimental (b) collector current pulse in the case of trapping type interaction with a decelerating axial field (horizontal scale: 200 ns/div; vertical scale: 1 μA/div).

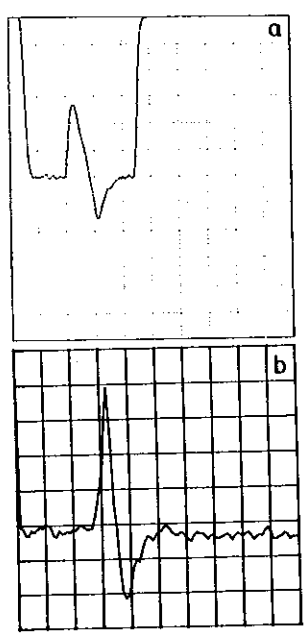

Fig. 16. Theoretical (a) and experimental (b) collector current pulse in the case of trapping type interaction with an accelerating axial field (horizontal scale: 200 ns/div; vertical scale: 1 μA/div).

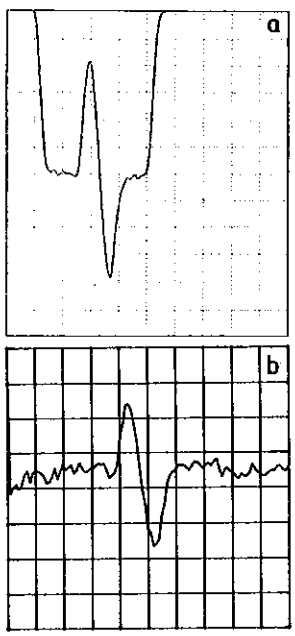

Fig. 17. Theoretical (a) and experimental (b) collector current pulse in the case of PAD type interaction with a decelerating axial field (horizontal scale: 200 ns/div; vertical scale: 1 μA/div).

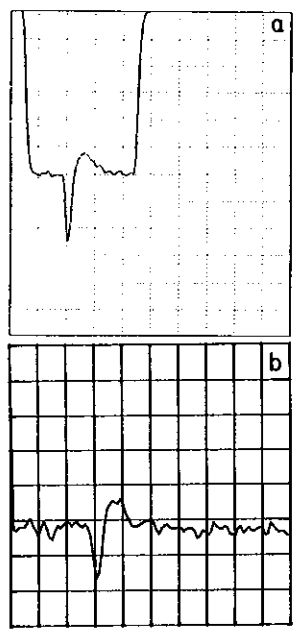

Fig. 18. Theoretical (a) and experimental (b) collector current pulse in the case of PAD type interaction with an accelerating axial field (horizontal scale: 200 ns/div; vertical scale: 1 μA/div).

user. Later the electrons are simulated passing through a short tube. The potential of this tube is used to filter out electrons below a certain energy. The electrons emerging from this tube enter a low potential drift tube that is used to disperse timewise electrons with different energies. Finally these electrons are collected and then transformed into a current pulse that is later passed through a five pole digital filter with a bandwidth of 20 MHz similar to the one used by the digital scope that is used to collect the experiment results.

The results obtained from these simulations show good agreement with the experimental results as can be seen from figs. 15 and 16 for a case in which the synchronism adjusted for trapping in a decelerating and accelerating field respectively, and from figs. 17 and 18 for the case in which synchronism was adjusted for PAD in a decelerating and accelerating field respectively. It should be noted here that any change in one of the trapping or PAD properties appreciably changes the shape and also the timing of the current pulse.

References

[1] Norman M. Kroll, Philip L. Morton and Marshall N. Rosenbluth, IEEE J. Quantum Electron. QE-17 (1981) 1436.
[2] R.Z. Olshan, S. Ruschin, A. Gover, H. Kleinman, B. Lissak and Z. Sheena, Nucl. Instr. and Meth. A259 (1987) 119.
[3] Z. Sheena, S. Ruschin, A. Gover and H. Kleinman, submitted to IEEE J. Quantum Electron.
[4] M.N. Rosenbluth, B.N. Moore and H. Vernon Wong, IEEE J. Quantum Electron. QE-21 (1985) 1026.
[5] R.Z. Olshan, A. Gover, S. Ruschin and H. Kleinman, Phys. Rev. Lett. 58 (1987) 483.